

# Sparse group LASSO and nonlinear machine learning for frequency-feature optimization in noninvasive blood glucose monitoring via bioimpedance spectroscopy

Cite as: Rev. Sci. Instrum. 96, 074702 (2025); doi: 10.1063/5.0251837

Submitted: 5 December 2024 • Accepted: 11 June 2025 •

Published Online: 1 July 2025



View Online



Export Citation



CrossMark

Zhongwei Lu,<sup>1,2</sup> Tian Zhou,<sup>3</sup> Cong Hu,<sup>1,2,4,a</sup> Chuanpei Xu,<sup>1,2</sup> Shike Long,<sup>5</sup> Shaorong Zhang,<sup>3</sup> and Benxin Zhang<sup>1</sup>

## AFFILIATIONS

<sup>1</sup> School of Electronic Engineering and Automation, Guilin University of Electronic Technology, Guilin 541004, China

<sup>2</sup> Guangxi Key Laboratory of Automatic Detecting Technology and Instruments, Guilin 541004, China

<sup>3</sup> School of Electronic Information and Automation, Guilin University of Aerospace Technology, Guilin 541004, China

<sup>4</sup> Guangxi Key Laboratory of Brain-inspired Computing and Intelligent Chips, Guangxi Normal University, Guilin 541004, China

<sup>5</sup> School of Aeronautics and Astronautics, Guilin University of Aerospace Technology, Guilin 541004, China

<sup>a</sup>Author to whom correspondence should be addressed: [hucong@guet.edu.cn](mailto:hucong@guet.edu.cn)

## ABSTRACT

Diabetic patients need to test their blood glucose levels (BGL) frequently; however, traditional methods of blood collection and testing cause great pain to patients. In order to improve the quality of life of patients, this paper develops a noninvasive, portable, and continuous monitoring blood glucose detection system, which uses the latest bioimpedance integrated circuit to obtain the bioimpedance spectrum (BIS) of the inner forearm of the human body. The obtained BIS covers most of the frequencies up to 1 MHz. A BGL estimation model is developed using sparse group least absolute shrinkage and selection operator combined with a Gaussian kernel function support vector regression to select the optimal frequencies and features for BIS. The correlations between different frequencies and features and BGL are investigated. We test our system on a collected dataset of clinical subjects, and the results show that the average mean absolute relative difference for all subjects is 9.90%, the root mean square error is 14.81 mg/dl, and the mean absolute error is 11.75 mg/dl. 100% of the estimates fall in zones A and B of the Clarke error grid. Preliminary results show that the use of BIS integrated circuits in combination with machine learning techniques promises to enable portable, noninvasive, continuous monitoring of BGLs.

Published under an exclusive license by AIP Publishing. <https://doi.org/10.1063/5.0251837>

05 July 2025 07:44:50

## I. INTRODUCTION

Diabetes is a common chronic disease in humans, and BGL is an important indicator for managing diabetes. Traditional invasive blood glucose monitoring requires finger pricking to obtain BGLs, which not only brings financial pressure but also causes pain and a risk of wound infection for patients.<sup>1</sup> Therefore, there is an urgent need for a noninvasive BGL estimation technique that is both accurate and economical as an alternative to invasive methods.

Currently, many technologies are used for noninvasive blood glucose detection. Chen *et al.*<sup>2</sup> used photoplethysmography (PPG)

to detect blood glucose concentration and achieved high accuracy through innovative signal preprocessing methods and multi-view feature fusion networks. Reference 3 developed wearable devices using red and near-infrared light, which can continuously monitor BGLs. However, the aforementioned optical methods are susceptible to interference from skin color, environmental factors, and background signals. Literature<sup>4</sup> uses microwave techniques to measure glucose concentration; they use a designed antenna to perform human experiments in the frequency band of a few GHz, resulting in a MARD of 5.9%. However, the vector network analyzer for microwave measurements is expensive and difficult to

miniaturize. In addition, tears<sup>5</sup> and sweat<sup>6</sup> have been used to detect glucose; however, the correlation between these blood substitutes and blood glucose concentration is not strong and lacks the support of underlying theory.<sup>7</sup> In contrast, BIS has the advantages of small and inexpensive equipment, easy data acquisition, and a solid theoretical foundation. Studies have been conducted to design portable, noninvasive glucose detection instruments based on BIS.<sup>8</sup>

The basic principle of BIS is to inject low-frequency alternating current into biological tissues to measure the changes in electrical impedance of the red blood cell membrane, intracellular fluid, and extracellular fluid caused by changes in blood glucose concentration.<sup>9</sup> BIS typically sweeps over a wide frequency band and can obtain bioimpedance data at a large number of frequency points. This leads to two questions: how should the correlation between bioimpedance and BGL be determined at different frequency points? How can different frequencies and features be combined to achieve accurate and robust noninvasive BGL estimation?

On one hand, existing studies have demonstrated a high correlation between bioimpedance and BGLs in the frequency range of several hundred kHz. Literature<sup>10</sup> measured bioimpedance in the range of 100 Hz to 30 MHz using a complex impedance analyzer and found that bioimpedance in the frequency range of hundreds of kHz had the highest correlation with BGL. Literature<sup>11</sup> directly measured the electrical impedance of blood and found that the electrical impedance of blood samples with different glucose concentrations changed significantly in the frequency range of 100 Hz to 1 MHz. Subsequent attempts have been made to model BGL estimation by selecting frequencies or combinations of frequencies with high correlation with blood glucose concentration using various feature selection methods. Literature<sup>12</sup> set the sweep range from 3 to 100 kHz, selected the bioimpedance of the top 20 frequencies with the highest Pearson correlation coefficients with BGLs as the features, and then used principal component analysis for dimensionality reduction. However, it is well known that there is a nonlinear relationship between bioimpedance and BGL that has not yet been fully clarified, and the use of Pearson correlation coefficients, which is a linear method for selecting frequencies, could not fully capture the complex nonlinear relationship between changes in blood glucose concentration and bioimpedance. Literature<sup>13</sup> and<sup>14</sup> utilized the Akaike information criterion and backward elimination method to select the optimal frequency combinations from 0.1 to 25 MHz and 1 kHz to 100 MHz, respectively. However, the Akaike information criterion is not applicable to the case of an excessive number of frequencies and features in the BIS. The backward elimination method, in addition to being computationally expensive, may not allow for the correct selection of important variables in the case of multiple covariates,<sup>15</sup> which can be a problem in BIS since the multiple frequencies may be correlated with each other. There is also some literature<sup>16,17</sup> that does not consider the correlation with BGL after selecting the frequencies based on domain knowledge, which may lead to irrelevant physiological information interfering with the modeling. The correlation between frequencies and BGL may be different for different individuals.

On the other hand, bioimpedance can be described by four characteristic parameters: real part, imaginary part, magnitude, and phase. The real part is mainly due to the water content in the body and reflects the electrical resistance characteristics in biological tissues. The imaginary part is mainly due to the capacitance generated

by cell membranes, and the magnitude and phase can be derived from the real and imaginary parts.<sup>18</sup> Although it is well established that changes in BGLs alter these four features, the extent to which they correlate with BGLs is not clear. Therefore, it is necessary to select features with larger contributions to participate in the estimation of BGL, which can avoid feature redundancy and reduce the interference of irrelevant information.

Based on the above analysis, we first use a portable bioimpedance sensor to measure BIS within the range of 1 MHz for modeling BGL estimation. Then, to address the issues of how to determine the degree of correlation between different frequencies and BGLs and how to combine different frequencies and features to achieve accurate and robust estimation of BGLs, we propose to use sgLASSO to select the frequencies and four features of the BIS. This realizes the automatic selection of the frequencies and features and ensures the interpretability of the model. Meanwhile, in order to solve the problem that linear models are mainly suitable for feature selection of linear relationships and cannot directly capture the nonlinear characteristics of the data, we use a nonlinear machine learning regression algorithm to evaluate the frequencies and features selected based on sgLASSO, which indirectly realizes the capture of nonlinear characteristics. Finally, the same nonlinear regression algorithm is used to model the final BGL estimates.

This paper is organized as follows: Sec. II reviews the theoretical basis of noninvasive blood glucose detection based on BIS; Sec. III describes the new BIS data preprocessing method and the newly proposed algorithm framework; Sec. IV describes the experimental devices and the data acquisition process; experimental results analysis and discussion are reported in Secs. V and VI, respectively; finally, Sec. VII concludes this study.

## II. THEORETICAL BASIS

Figure 1 shows a schematic diagram of the principle of measuring bioimpedance using the four-electrode method. This method uses two current electrodes to inject a low-frequency, alternating weak current into human tissue, and two receiving electrodes, positioned between the two current electrodes, to measure the voltage difference. The four-electrode method eliminates the interfacial impedance between the skin and the sensor compared to the two-electrode method, thereby mitigating measurement errors due to interfacial effects.<sup>19</sup> Currents of different frequencies propagate through tissues such as skin and blood vessels. The flow of different substances inside and outside the cell membrane when blood glucose concentration changes, and the equivalent circuit model of a single red blood cell, are also shown.

Changes in blood glucose concentration can alter electrical conduction in organisms. Changes in glucose concentration in the blood can alter the activity of transport proteins on the cell membrane. The process of transporting glucose from the outside of cells to the inside of cells through glucose transporters on the cell membrane, and using it as an energy substance for cell utilization, can change the permeability and dielectric properties of the cell membrane, while other substances (such as proteins and fats) do not possess this property.<sup>20</sup> The elevation of glucose levels in the bloodstream not only increases plasma resistivity but also leads to a reduction in sodium ion concentration and an increase in potassium ion concentration within red blood cells. This, in turn, impacts the conductivity of

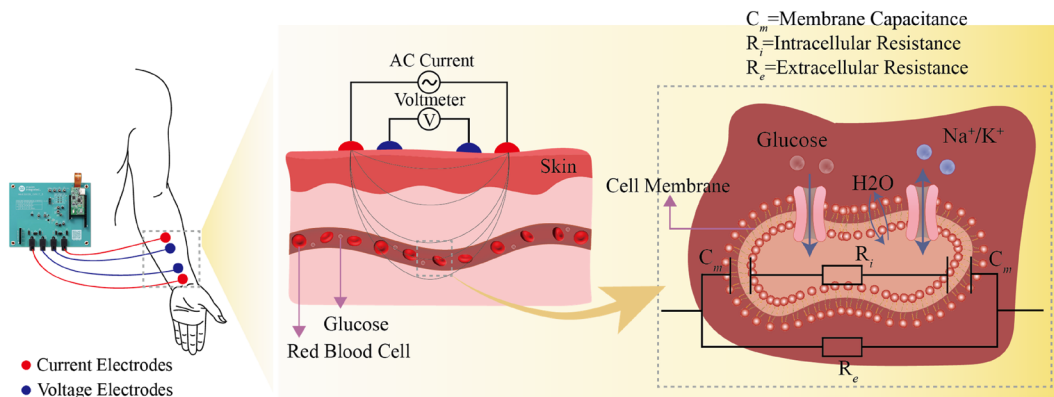


**FIG. 1.** Schematic diagram of the theoretical principle of noninvasive BGL estimation by the BIS method.

red blood cell membranes, resulting in corresponding alterations in the macroscopic dielectric constant of human tissues.<sup>21</sup> In addition, because blood and tissue cells respond specifically to different concentrations of glucose, changes in blood glucose concentration alter the electrical properties of perivascular tissues, and the electrolyte balance in the dermis will also change, leading to changes in electrical conduction.<sup>9</sup>

Researchers build human body impedance models consisting of resistors and capacitors.<sup>22–26</sup> The model equates intracellular and extracellular fluids, as electrolytes, to resistors, and cell membranes and other membrane-like tissues to capacitors.<sup>27</sup> Equation (1) describes the tissue as a function of conductivity  $\sigma$  and dielectric constant  $\epsilon$  according to the simplest model of impedance:<sup>28</sup>

$$Z = \frac{1}{G + jwC} = \frac{d/A}{\sigma + jw\epsilon}. \quad (1)$$

In Eq. (1),  $G$  and  $C$  denote the conductance and capacitance of the model, respectively,  $d$  and  $A$  are the thickness and cross-sectional area of the tissue sample, and  $w$  is the angular frequency of the signal injected into the tissue. From the equation, the impedance of tissue depends on the frequency of the signal. Low-frequency current only flows through extracellular fluid, contributing to conductivity, while high-frequency current penetrates the cell membrane and flows through both intracellular and extracellular fluids, contributing to both conductivity and capacitance.<sup>27</sup> The low-frequency current penetrates deeper into tissue, while the higher-frequency current penetrates cells, so its path is shallower and shorter.<sup>29,30</sup> Therefore, measuring bioimpedance within a certain frequency range can obtain information on multiple different tissues through which the current passes.<sup>8</sup> It has been shown that the injection of AC currents below 1 MHz into biological tissues can reflect counterion effects near the membrane surface, active cell membrane effects and gated channels, as well as passive cell membrane capacitance and intracellular organelle membrane properties.<sup>31</sup>

In summary, noninvasive BGL estimation can be achieved by measuring the BIS of human tissue at different frequencies within 1 MHz.

### III. ALGORITHM FRAMEWORK DESIGN BASED ON BIS AND sGLASSO

The overall data processing framework of the proposed method is shown in Fig. 2. The bioimpedance signals at multiple frequencies are collected using the frequency sweep method, while the reference BGL is obtained using the invasive method of blood collection by pricking the finger. The multi-frequency bioimpedance signals are first preprocessed to construct the BIS. Feature computation is used to construct the complete feature set, and then feature fusion is performed according to preset rules to fit the algorithmic framework. These data are then co-assembled with the reference BGL to form a dataset and divided into a training set and a test set. The training set is used to train the machine learning regression model, and the test set is used to validate the best-trained model.

#### A. Data preprocessing

Figures 3(a)–3(d) show the real and imaginary components of the bioimpedance signals acquired at 50 and 800 kHz frequencies. As can be seen from Figs. 3(a) and 3(b), there is a large fluctuation in the initial stage of the signal, which then reaches a relatively stable state. This is caused by the sensor's settling time. Therefore, to reduce noise interference, we set the number of sampling points to 64, delete the first 32 sampling points of the signal, and take the average of the last 32 sampling points. After performing the same processing on the signal at each frequency point, the BIS shown in Figs. 3(e) and 3(f) is formed. To obtain the complete bioimpedance features, we calculate the corresponding magnitude and phase features based on the real and imaginary parts of the obtained bioimpedance. The calculation formulas are shown in (2) and (3):

$$Mag = \sqrt{I^2 + Q^2}, \quad (2)$$

$$Pha = \arctan\left(\frac{Q}{I}\right), \quad (3)$$

where  $I$ ,  $Q$ ,  $Mag$ , and  $Pha$  denote the real part, imaginary part, magnitude, and phase of the bioimpedance, respectively. Next, we concatenate the four features at the same frequency and concatenate

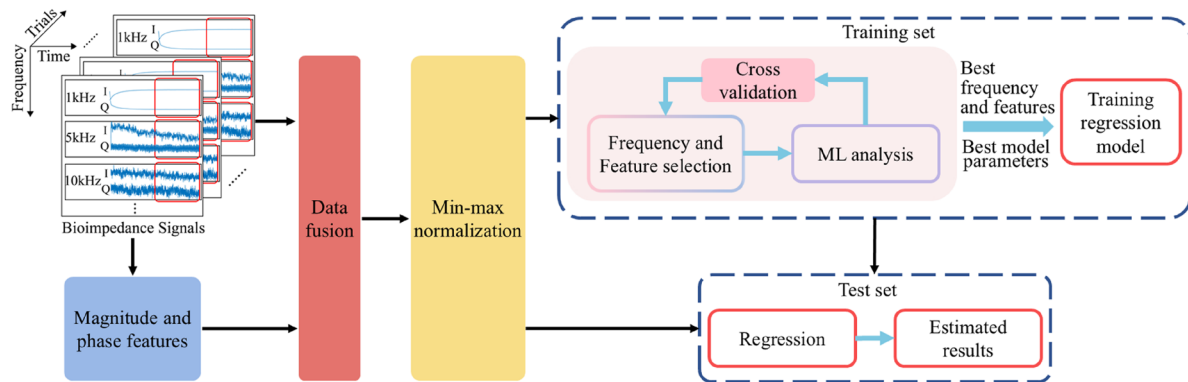


FIG. 2. Overall framework for data processing.

the features of all frequencies into a feature vector in order. This is done to adapt to the proposed algorithm framework. After performing the same preprocessing on all the BIS samples, we obtain the complete dataset, which is then divided into training and test sets. Finally, the feature sample matrix of the training set is normalized using max–min normalization and applied to the test set. The formula for normalization is shown in (4):

$$X_j^i = \frac{S_j^i - \min(S^i)}{\max(S^i) - \min(S^i)}, \quad (4)$$

where  $\max(s^i)$  and  $\min(s^i)$  represent the maximum and minimum values of the eigenvector, respectively, and  $\mathbf{X} = (\mathbf{x}_1, \mathbf{x}_2, \dots, \mathbf{x}_N)^T \in R^{N \times P}$  represents the bioimpedance feature sample matrix.

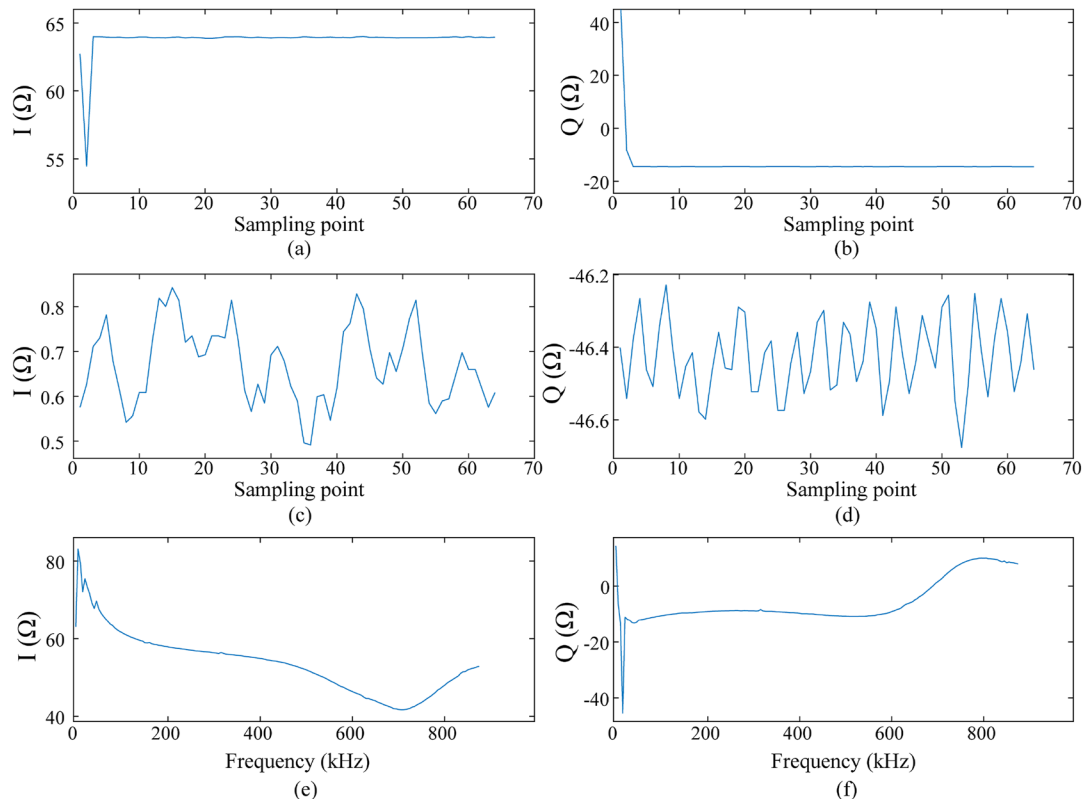


FIG. 3. The obtained bioimpedance signals. [(a) and (b)] are the real and imaginary signal components of the bioimpedance at 50 kHz; [(c) and (d)] are the real and imaginary signal components of the bioimpedance at 800 kHz; and [(e) and (f)] are the real and imaginary signal components of a sample of the bioimpedance spectrum, respectively.

## B. Frequency and feature selection and regression analysis

Although it has been demonstrated that bioimpedance has a high correlation with BGLs in the frequency range of hundreds of kHz. However, bioimpedance also correlates with physiological information such as body water, fat, and muscle content. Considering that different frequencies measure different tissue depths and mainly respond to different physiological characteristic information, the combination of multiple frequencies implies the combination of multiple physiological characteristics. Therefore, it is necessary to exclude the interference of irrelevant information and select the frequencies and features that contribute most to the estimation of BGLs.

The least absolute shrinkage and selection operator (LASSO)<sup>32</sup> can be used for high-dimensional feature selection because it includes the  $l_1$ -norm with sparsity-inducing ability, and has been used to estimate BGL with good results.<sup>33,34</sup> The specific mathematical model is as follows:

$$\min_w \frac{1}{2} \|y - Xw\|_2^2 + \lambda \|w\|_1, \quad (5)$$

where  $y = [y_1, y_2, \dots, y_N]^T$  is the sample label,  $w \in R^P$  is the feature weight,  $\|w\|_1 = \sum_{k=1}^P |w_k|$ ,  $|w_k|$  denotes the absolute value of the  $k$ th element of  $w$ , and  $\lambda > 0$  is a regularization parameter. Since  $w$  represents the importance of the corresponding features, the model built using LASSO has good interpretability and is also convenient for data visualization. However, LASSO only achieves ordinary unstructured sparsity. To analyze data with group structure, the gLASSO model was proposed,<sup>35,36</sup> and the specific mathematical model is as follows:

$$\min_w \frac{1}{2} \|y - Xw\|_2^2 + \lambda \|w\|_{2,1}, \quad (6)$$

where  $\|w\|_{2,1} = \sum_{g=1}^G \|w_{[g]}\|_2$ ,  $w_{[g]}$  is the  $g$ th group of  $w$ , and  $G$  is the total number of groups. By introducing the  $l_{2,1}$ -norm, it can exclude feature groups with group weights of 0 or close to 0.

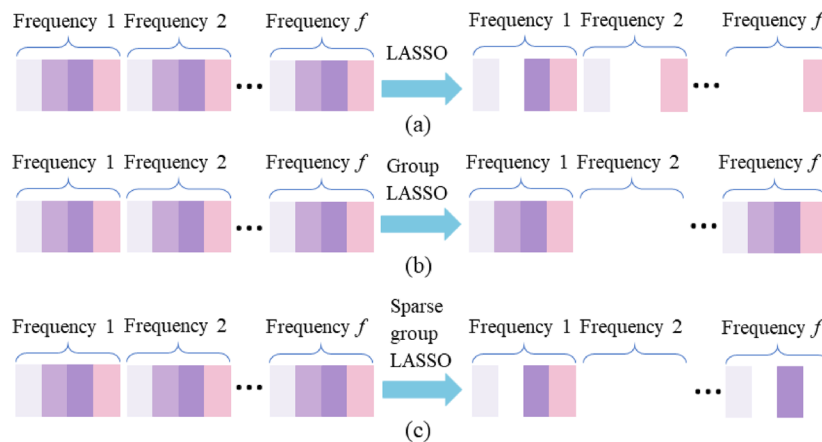


**FIG. 4.** Schematic diagram of frequency and feature selection: (a) LASSO only selects features. (b) gLASSO either selects all features of a frequency or none. (c) sgLASSO considers both frequency redundancy and feature redundancy.

However, gLASSO does not consider feature redundancy within groups.

sgLASSO<sup>37,38</sup> combines the  $l_1$ -norm and  $l_{2,1}$ -norm to achieve both between-group and within-group sparsity. The specific mathematical model is as follows:

$$\min_w \frac{1}{2} \|y - Xw\|_2^2 + \lambda_1 \|w\|_{2,1} + \lambda_2 \|w\|_1, \quad (7)$$

where  $\|w\|_{2,1}$  is the same as the second term of Eq. (6) and  $\|w\|_1$  is the same as the second term of Eq. (5). The principle diagram of frequency and feature selection based on sgLASSO proposed in this paper is shown in Fig. 4. Considering that each frequency point in the BIS includes four features—real part, imaginary part, magnitude, and phase—these feature variables belonging to the same frequency naturally form group variables. Therefore, to fully utilize the prior information of group structure, we select the frequencies and features that contribute most to modeling based on sgLASSO.

In terms of regression analysis, the nonlinearity of the sensor components and the complexity of the physiological system being measured, as well as the interaction between the two, indicate a nonlinear relationship between the measured BIS and BGL.<sup>39–41</sup> Compared to linear models, nonlinear models are less affected by noise and outliers in the data. Therefore, nonlinear models such as neural networks with nonlinear activation functions, RF, and Gaussian kernel SVR are expected to have good estimation accuracy when estimating BGL. However, due to ethical and cost constraints, the data collected in this study form a small-sample dataset that would be difficult to adjust and optimize if deep learning methods were used. Traditional machine learning models such as SVR, KNN, and RF are more suitable for use on small-sample datasets.

In summary, this paper proposes to combine sgLASSO and nonlinear machine learning regression modeling to achieve simultaneous frequency and feature selection of BIS. This approach takes full advantage of the linear regression technique, in which the norm penalty term can select features, and at the same time uses a nonlinear model to evaluate the effect of frequency and feature selection, indirectly capturing nonlinear features. The specific implementation process is shown in Algorithm 1.

**ALGORITHM 1.** Proposed BGL estimation algorithm.

---

**Input:** Let  $X$  denotes the bioimpedance feature matrix and  $y$  denotes the blood glucose level vector.

**Output:** Optimal feature set and regression model

- 1: Given  $\lambda_1, \lambda_2 \in \{2^{-5}, 2^{-4.8}, \dots, 2^5\}$ ,  $error = inf$ .
- 2: For  $i = 1$  to  $length(\lambda_1)$
- 3: For  $j = 1$  to  $length(\lambda_2)$
- 4: Calculate  $w$  according to (7).
- 5: Select feature index  $|w| > 0$  and get the feature subset.
- 6: Train a regression model using ten-fold cross-validation and get  $rmse$ .
- 7: If  $rmse < error$
- 8: Save feature index and regression model parameters
- 9: End if
- 10: End for
- 11: End for

---

**C. Evaluation metrics**

The design of the evaluation model is crucial for the construction of an efficient machine learning model, while appropriate evaluation metrics are essential for accurately quantifying the performance of the algorithm. In this paper, mean absolute relative difference (MARD), root mean square error (RMSE), and mean absolute error (MAE) are used to evaluate the model performance, as follows:

$$MARD = \frac{1}{N} \sum_{i=1}^N \frac{|y_{prediction}^i - y_{label}^i|}{y_{label}^i} \cdot 100\%, \quad (8)$$

$$RMSE = \sqrt{\frac{\sum_{i=1}^N (y_{prediction}^i - y_{label}^i)^2}{N}}, \quad (9)$$

$$MAE = \frac{1}{N} \sum_{i=1}^N |y_{prediction}^i - y_{label}^i|, \quad (10)$$

where  $y_{prediction}$  is the estimated BGL vector for  $N$  samples and  $y_{label}$  is the reference BGL vector.

In addition to evaluating the model statistically, the clinical impact of estimation bias should be considered. The Clarke Error Grid (CEG) is used to evaluate the clinical accuracy of blood glucose meters and has become the gold standard.<sup>42</sup> This grid consists of five regions. Zone A indicates that the estimated BGL is within 20% of the reference BGL. The error in Zone B exceeds 20%, but these estimates can still support meaningful medical diagnoses. Therefore, zones A and B are considered clinically acceptable. When the predicted BGL value falls into the C, D, or E zones, the estimated result is not clinically acceptable. These values may lead to clinically meaningless or even dangerous medical decisions.<sup>41</sup>

**IV. DATA ACQUISITION****A. Construction of software and hardware platforms**

In this paper, the MAX30009EVKIT (Maxim Integrated, San Jose, CA, USA) was used to measure bioimpedance. Prior to human

experiments, the device was validated using electrical models to ensure measurement accuracy. A precise resistor ( $50 \Omega$ ), close to the impedance of typical human forearm tissue, was used for calibration. The measured impedance magnitude and phase errors were confirmed to be close to  $0.1 \Omega$  and  $0.1^\circ$ , respectively, aligning with the manufacturer's specifications.<sup>43</sup> It is more than 100 times less expensive than similar impedance analyzers and is available in a  $2 \times 2$  mm wafer-level package. Moreover, it boasts ultra-low power consumption, requiring only  $250 \mu\text{W}$  at  $1.8 \text{ V}$ . Each electrode pin on the evaluation board has a DC blocking capacitor that prevents DC current from being driven into the patient's body. These advantages make it a highly competitive option for portable noninvasive blood glucose meters.

The MAX30009EVKIT is accompanied by evaluation software, and its microcontroller performs Bluetooth communication to transmit data to a personal computer.

**B. Human experiment**

According to the typical application example of the MAX30009, this study used a four-electrode measurement configuration in low-noise mode, with all onboard digital and analog filters set to bypass. To measure bioimpedance at all frequencies available to the hardware, the excitation current was set to  $64 \mu\text{A}$ . Four "wet" Ag/AgCl gel electrodes were used. To reduce systematic errors and improve resolution, the electrodes were placed on the medial side of the left forearm, where the skin is thin and the arterial blood supply is abundant.<sup>12,39</sup> To allow the different frequency components of the current to propagate at different depths within the tissue and to reduce computation and sweeping time due to highly similar bioimpedance at adjacent frequency points, the measurement frequency range was set from 1 to  $875 \text{ kHz}$ , with an interval of  $5 \text{ kHz}$ . This study received ethical approval from Guilin University of Electronic Technology (ID: GUET-2024-0801).

As shown in Fig. 5, human experiments were conducted on volunteers. We recruited nine volunteers and conducted a total of 18 oral glucose tolerance test (OGTT) experiments. All participants were healthy college students aged between 21 and 30 years. They fasted for 8 h before the experiment began. During data collection,

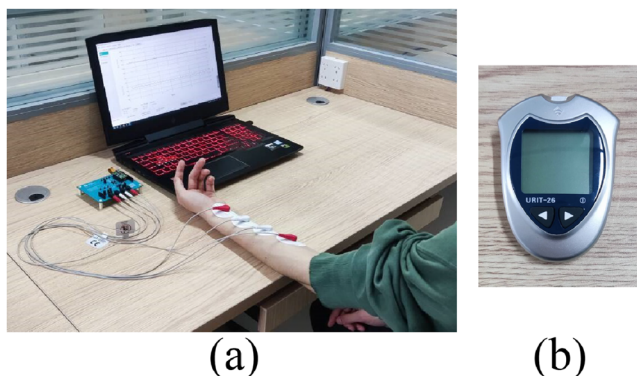


**FIG. 5.** Human experiment devices. (a) BIS were acquired using a MAX30009EVKIT and the data were saved to a laptop. (b) Reference BGLs were collected using a commercial invasive glucometer.

subjects were asked to sit in a comfortable chair, remain still, and keep their whole-body muscles relaxed to avoid motion artifacts during anthropometry. The room temperature was maintained at  $26 \pm 1^\circ\text{C}$ . First, reference BGLs and BIS were collected in the fasting state, followed by the oral intake of a glucose solution (120 g glucose). Over the next 3 h, reference BGLs were measured every 5 min using a commercial invasive blood glucose meter (URIT-26), and BIS were collected at the same time. The distance between electrodes was kept consistent for each measurement. Each subject completed two OGTT experiments. Each OGTT recorded 37 measurements, including one fasting measurement. Each OGTT was processed separately. All samples from each OGTT were randomly divided into an 80% training set and a 20% test set. It should be noted that, to fully characterize system performance, all data from all subjects were included, and no sample deletion was performed. We will analyze the experimental results in detail in later chapters.

## V. EXPERIMENT RESULTS

## A. Model parameter settings

In this paper, sgLASSO was used for frequency and feature selection, with LASSO and gLASSO used for comparisons, implemented using the SLEP toolbox. The set of regularization

**TABLE I.** Performance comparison of different methods. Boldface denotes the proposed method and its performance.

Method	MARD (%)	RMSE (mg/dl)	MAE (mg/dl)
SVR	17.42	25.19	20.67
LASSO+SVR	11.21	16.89	13.49
gLASSO+SVR	12.02	18.01	14.19
<b>sgLASSO+SVR</b>	<b>9.90</b>	<b>14.81</b>	<b>11.75</b>

parameters selected was all  $\{2^{-5}, 2^{-4.8}, \dots, 2^{4.8}, 2^5\}$ . The machine learning regression algorithm used was SVR, implemented using the Statistical and Machine Learning Toolbox. The kernel function selected was the Gaussian kernel function, with all other parameters set to the default settings of the toolbox. K-Nearest Neighbors and Random Forest were also used for comparison. The number of neighbors for KNN was set to 5, using Euclidean distance. The number of decision trees for RF was set to 10. The model training procedure is shown in Algorithm 1. It should be noted that LASSO and gLASSO have only one regularization parameter, whereas sgLASSO has two. All experiments were performed using MATLAB R2024a software.

## B. Estimation results

**Table I** lists the performance comparison of the results obtained using LASSO, gLASSO, and sgLASSO for frequency and feature selection, with SVR as the regression algorithm, and directly using SVR without any frequency and feature selection algorithm. From the table, it can be seen that the optimal performance was obtained using sgLASSO for frequency and feature selection. The average MARD for all experiments is 9.90%, and the average RMSE is 14.81 mg/dl. The average MAE is 11.75 mg/dl. The results obtained using both LASSO and gLASSO were worse than those using sgLASSO, and the worst performance was obtained without any feature selection method. We also performed the same experiments using KNN and RF, and the results showed that both performed worse than SVR. Due to space constraints, we do not provide the detailed experimental results here.

The MARD, RMSE, and MAE for all 18 OGTT groups are presented in Fig. 6. As seen in the figure, most groups have small estimation errors, with the MARD mostly <10%. However, we observed

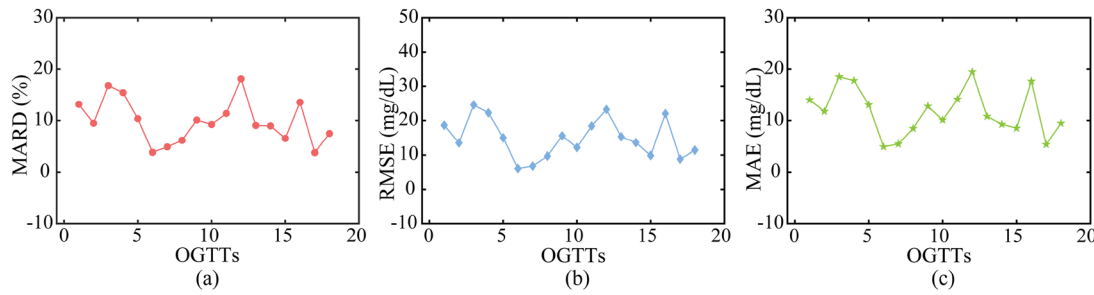


**FIG. 6.** Performance of all 18 OGTT groups: (a) the mean absolute relative difference (MARD), (b) the root mean square error (RMSE), and (c) the mean absolute error (MAE).

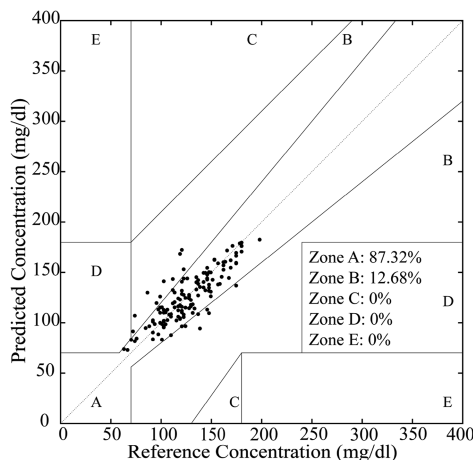


**FIG. 7.** Clarke error grid analysis of the estimation results obtained using sgLASSO+SVR.

the existence of a few groups with relatively large estimation errors, such as groups 3, 4, 12, and 16, all of which had RMSE values above 20 mg/dl. We will analyze this in the discussion.

Figure 7 shows the Clarke error grid analysis plot of the BGL estimates obtained using the proposed method. From the figure, it can be seen that 100% of the estimates fall into clinically acceptable zones A and B, with 87.32% of the estimates fall into zone A. This implies that the BGL estimates obtained using our system are clinically reliable and meaningful for guiding medical practice.

### C. Comparison with other noninvasive BGL estimation systems

To demonstrate the advantages of the system we have developed in this paper, it was compared with other state-of-the-art noninvasive glucose detection techniques. It is important to note that all comparisons are based on human experiments, with personalized models trained for each subject, as shown in Table II. The performance in the literature<sup>44</sup> is comparable to our results, but this work involves a smaller number of subjects and only reports experimental results for one subject. In addition, such noninvasive glucose detection systems using vector network analyzers are more difficult to miniaturize, whereas the bioimpedance sensor used in

this paper is more suitable for portable applications. Literature<sup>45</sup> reported worse performance and used a narrower range of BGLs for testing, although the work collected data from the same subject for several days, which will be the subject of our future work. For fairness in comparison, for literature,<sup>12</sup> we only consider the results of the BIS part of this work. The results show that our system not only achieves a lower estimation error but also tests a wider range of BGLs.

In summary, the method proposed in this paper achieves high estimation accuracy and clinical reliability, which provides great confidence for the realization of portable noninvasive BGL detection systems.

## VI. DISCUSSION

### A. Analysis of frequency and feature selection results

We model each OGTT experiment separately because we want to exclude the interference of individual differences and represent as thoroughly as possible the correlation between different frequencies and features of bioimpedance and BGLs. We use one of the subjects as an example to analyze the results of frequency selection and feature selection separately. Figure 8(a) shows the frequencies and features selected for one of the OGTTs using our proposed method. From the frequency selection results, the algorithm excludes most of the frequencies and selects only six frequency points with the highest contribution, from 1 to 5 kHz and from 650 to 700 kHz. This combination of low and high frequencies implies a combination of different penetration depths of the current into biological tissues, reflecting the physiological characteristics of tissues at different depths. Moreover, since low-frequency currents such as 1 and 5 kHz do not easily penetrate the cell membrane, the bioimpedance of the extracellular fluid is mainly measured, whereas frequencies up to about 700 kHz easily penetrate the cell membrane and thus contain bioimpedance information of both intracellular fluid and the cell membrane. Therefore, this also means a combination of bioimpedance information from the cell membrane, intracellular fluid, and extracellular fluid.

From the results of feature selection, at 1 and 5 kHz, the real and magnitude features of bioimpedance were selected because the real part is mainly related to the resistance of the extracellular fluid, and the magnitude combines the information from both the real and imaginary parts and reflects the overall electrical properties of the tissue, including both resistive and capacitive properties. At 650–700 kHz, it is the imaginary part and the phase that are selected,

**TABLE II.** Comparison results with other methods.<sup>a</sup> Boldface denotes the proposed method and its performance.

Reference	Wang <i>et al.</i> <sup>44</sup>	Chowdhury <i>et al.</i> <sup>45</sup>	Nanayakkara <i>et al.</i> <sup>12</sup>	Ours
Modality	MW	PPG, EDA, ST, FL	BIS	<b>BIS</b>
BGLs range (mg/dl)	90–170	60–160	80–150	<b>60–200</b>
MARD (%)	9.74	12.57	11.25	<b>9.90</b>
RMSE (mg/dl)	13.32	17.26	...	<b>14.81</b>
MAE (mg/dl)	...	13.51	...	<b>11.75</b>
CEG A+B (A) (%)	...	99.43 (79.03)	100 (80)	<b>100 (87.32)</b>

<sup>a</sup>MW: microwave; PPG: photoplethysmogram; EDA: electrodermal activity; ST: skin temperature; FL: food log.

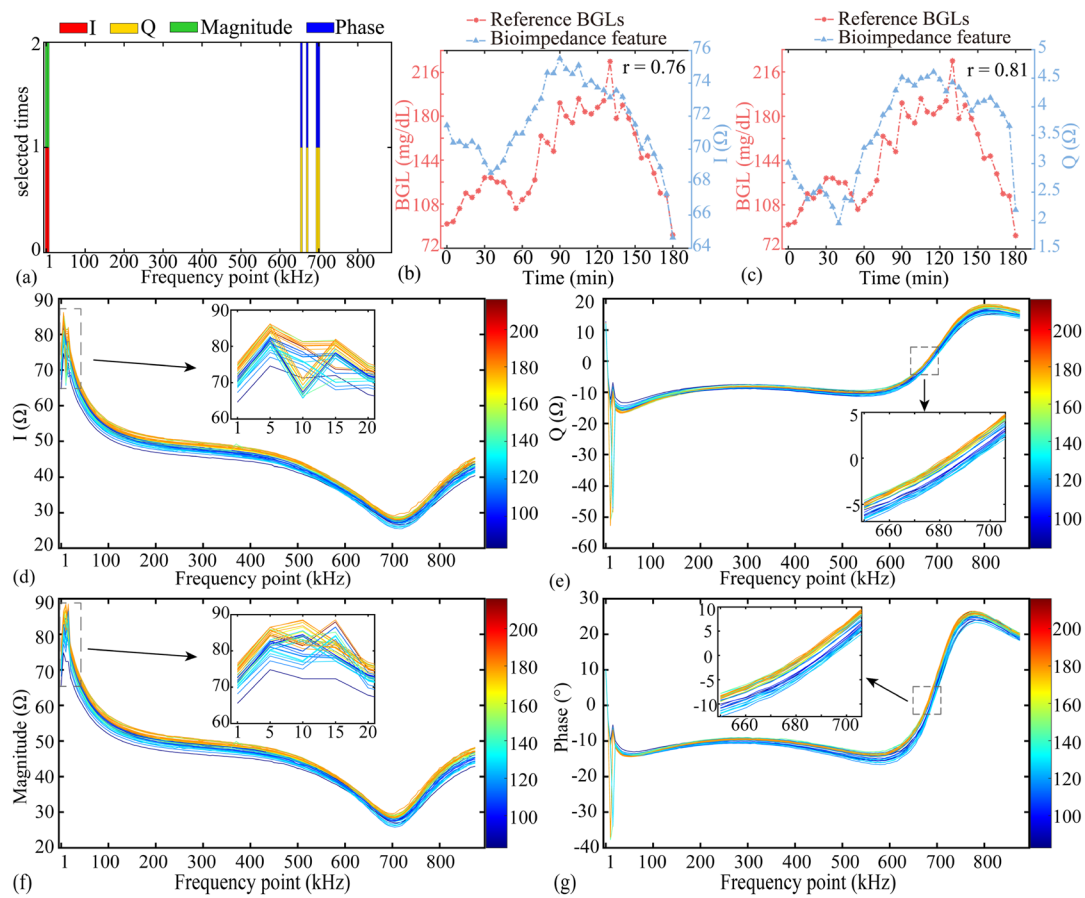


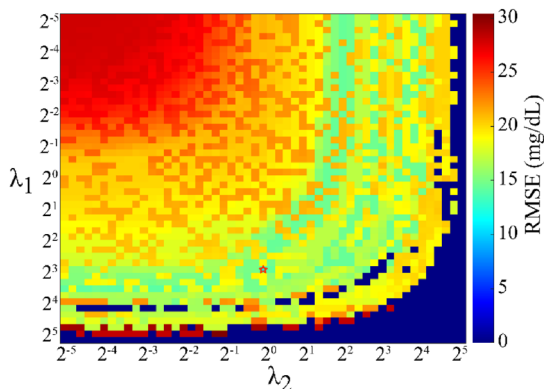
**FIG. 8.** Analysis of frequency and feature selection results in one experiment: [(a)] frequency and feature selection results; [(b) and (c)] the change of BGL over 180 min compared with the change in real part value at 1 kHz and imaginary part value at 700 kHz; [(d)–(g)] bioimpedance spectra of all samples and local magnifications, including the real part, imaginary part, magnitude, and phase, respectively.

where the phase mainly reflects the polarization state of the cell membrane and the activity of ion channels, and the imaginary part is related to the capacitive properties of the cell membrane, providing information about the integrity of the cell membrane and changes in the intracellular environment. Such frequency and feature selection results are consistent with the basic theory of bioimpedance, reflecting—at the cellular and tissue level—the altered physiological features resulting from changes in BGLs and revealed through bioimpedance changes. This also shows that the estimation results obtained using our system have high physiological interpretability.

Figures 8(d)–8(g) show the spectra of the real, imaginary, magnitude, and phase components in the range of 1–875 kHz and gives a localized magnification of the selected frequencies. It can be seen from the plots that the four impedance features of the selected frequencies have a clear distribution pattern at different blood glucose concentrations, which roughly show positive correlation. However, there are differences in the correlations at other frequencies. Figures 8(b) and 8(c) show the BGLs detected over 180 min after oral administration of a solution containing 120 g of glucose. The reference BGL is represented by the blue curve, and the red curves

represent the real part value of the impedance at a frequency of 1 kHz and the imaginary part value at 700 kHz, respectively. These show trends very similar to the upward and downward changes of the reference BGL, with correlation coefficients of 0.76 and 0.81, respectively, proving that the trends in measured bioimpedance values are mainly caused by changes in human blood glucose concentration. The experimental results indicate that the range of BGL changes was 90–220 mg/dl. The real part of bioimpedance varied between 64.5 and 75.5  $\Omega$ , while the imaginary part ranged from 1.9 to 4.6  $\Omega$ . Consequently, it can be inferred that for every 100 mg/dl increase in BGL, the real and imaginary parts of bioimpedance change by 8.46 and 2.08  $\Omega$ , respectively.

Although it has been demonstrated that our method can select the optimal frequency and feature combinations, the results of optimal frequency and feature selection vary from one OGTT to another due to individual differences, and the penalty parameter of sgLASSO needs to be carefully adjusted to ensure low estimation errors while achieving frequency and feature selection. For instance, in an OGTT experiment, as illustrated in Fig. 9, the RMSE is minimized ( $14.02 \text{ mg/dl}$ ) when  $\lambda_1 = 2^{2.8}$  and  $\lambda_2 = 2^0$ . In this case, a total of

FIG. 9. Cross-validation RMSE for different combinations of  $\lambda_1$  and  $\lambda_2$ .

10 features across three frequencies are selected, ensuring the model's simplicity.

Table III lists the average test results for all OGTTs when one of the real, imaginary, magnitude, or phase is used as feature, respectively. It can be seen that the estimation error is smaller and the number of selected frequencies is fewer when using fused features compared to using only a single feature. Fewer frequencies mean shorter sweep times and lower energy consumption, which is very meaningful for portable devices with extended endurance. Such results show that using a multi-frequency, multi-feature combination approach improves the accuracy of the model.

In addition, our algorithmic model has no overfitting problem. In the experimental results, the method had an average RMSE of 12.66 mg/dl in the training set, which indicates that it can accurately estimate BGLs from the training data. The average RMSE on the test set was 14.81 mg/dl, which is not much different from the training set, indicating that the method does not overfit the training set and can generalize well to new data.

## B. Limitations of the proposed method

From the results of the experiment, it can be seen that there exist several groups of OGTTs that have higher errors. This is due to the presence of explicit arm activity in the subjects during the data acquisition process, which can lead to muscle contraction, which in turn affects the impedance values. As shown in Fig. 10, there are a large number of abrupt changes in the impedance spectrum, which severely affect the algorithmic model's selection of the

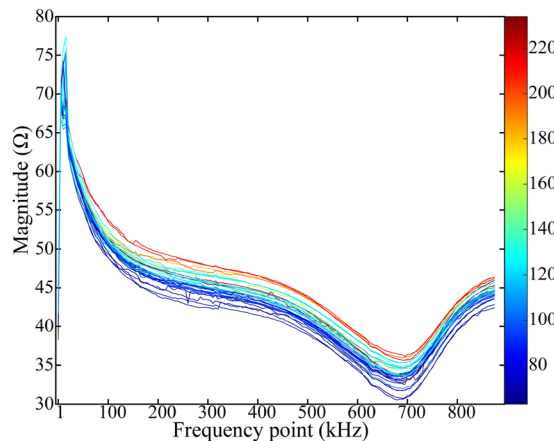


FIG. 10. Bioimpedance spectra collected in one OGTT experiment with the subject's arm in motion.

optimal frequency. Possible solutions include the use of accelerometers for motion compensation or applying algorithms such as data smoothing techniques for processing. Nevertheless, a positive correlation between BGL and bioimpedance magnitude is still clearly observed.

Our work has only demonstrated the reliability of the system for continuous measurements over a few hours. In future work, we plan to further evaluate the performance of the system by performing continuous BGL monitoring over a longer duration (e.g., one week).

The purpose of this work is to use the latest bioimpedance integrated circuit to collect the subject's body segment BIS and evaluate its correlation with BGL. Therefore, we conducted only within-subject experiments to exclude the influence of individual differences. If a universal model across subjects is to be established, more measurements from people of different ages and geographic regions must be obtained. These improvements will be addressed in future work.

## VII. CONCLUSION

In this paper, we use bioimpedance integrated circuits to realize noninvasive blood glucose detection based on BIS. Based on the *a priori* knowledge of the structure of BIS data, the use of sgLASSO with  $l_{2,1}$  and  $l_1$  paradigms is proposed to implement frequency and feature selection, while Gaussian kernel support vector regression is used to evaluate the selection results to indirectly capture the nonlinear information and to achieve optimal combinations of frequencies and features. The proposed method is validated on a clinical subject dataset. The results demonstrate that the optimal combination of frequencies and features can be selected using our method, that the selected features have high correlation with BGLs, and that using fused features further reduces frequency redundancy and improves estimation accuracy. Lower estimation errors and higher clinical reliability were observed compared to other within-subject modeling methods.

TABLE III. Comparison of experimental results of different features.

Feature	Number of frequencies	MARD (%)	RMSE (mg/dl)	MAE (mg/dl)
Real	7.61	11.70	17.52	14.12
Imaginary	9	12.43	17.84	13.80
Magnitude	7.17	11.28	17.71	13.74
Phase	7.67	11.38	16.44	13.36
Fusion feature	5.89	9.90	14.81	11.75

## ACKNOWLEDGMENTS

This work was supported by the National Natural Science Foundation of China (Grant No. 62171147), the Guangxi Key Laboratory of Automatic Detecting Technology and Instruments (Grant Nos. YQ23102 and YQ23210), the Guangxi Key Laboratory of Brain-inspired Computing and Intelligent Chips (Grant No. BCIC-23-K7), the Research Basic Ability Improvement Project for Young and Middle-aged Teachers of Guangxi Universities (Grant No. 2021KY0800), and the Guangxi Natural Science Foundation (Grant No. 2024GXNSFAA010512).

## AUTHOR DECLARATIONS

### Conflict of Interest

The authors have no conflicts to disclose.

### Ethics Approval

The Ethics Committee of Guilin University of Electronic Technology approved the project (ID: GUET-2024-0812), and informed consent was obtained from all participants.

### Author Contributions

**Zhongwei Lu:** Conceptualization (equal); Formal analysis (equal); Methodology (equal); Writing – original draft (equal). **Tian Zhou:** Software (equal); Writing – original draft (equal). **Cong Hu:** Funding acquisition (equal); Supervision (equal); Writing – review & editing (equal). **Chuanpei Xu:** Investigation (equal); Supervision (equal). **Shike Long:** Writing – review & editing (equal). **Shaorong Zhang:** Conceptualization (equal); Software (equal). **Benxin Zhang:** Conceptualization (equal); Software (equal).

## DATA AVAILABILITY

The data that support this study are available from the corresponding author upon reasonable request.

## REFERENCES

- <sup>1</sup>A. S. Bolla and R. Priefer, "Blood glucose monitoring- an overview of current and future non-invasive devices," *Diabetes Metab. Syndr.: Clin. Res. Rev.* **14**(5), 739–751 (2020).
- <sup>2</sup>S. Chen, F. Qin, X. Ma, J. Wei, Y.-T. Zhang, Y. Zhang, and E. Jovanov, "Multi-view cross-fusion transformer based on kinetic features for non-invasive blood glucose measurement using PPG signal," *IEEE J. Biomed. Health Inf.* **28**, 1982 (2024).
- <sup>3</sup>K. M A, R. Krishnamoorthy, R. Krishnamoorthy, S. Gogula, G. Chellamuthu, S. Muthu *et al.*, "Internet of Things enabled open source assisted real-time blood glucose monitoring framework," *Sci. Rep.* **14**(1), 6151 (2024).
- <sup>4</sup>Z. Wang, X. Xiao, Y. Pang, W. Su, and T. Kikkawa, "Noninvasive, intelligent blood glucose monitoring on fingertip using dual-band fusion and LSTM-R network," *IEEE Sens. J.* **24**, 3465 (2024).
- <sup>5</sup>W. Park, H. Seo, J. Kim, Y. M. Hong, H. Song, B. J. Joo, S. Kim, E. Kim, C. G. Yae, J. Kim *et al.*, "In-depth correlation analysis between tear glucose and blood glucose using a wireless smart contact lens," *Nat. Commun.* **15**(1), 2828 (2024).
- <sup>6</sup>C. Chen, Y. Fu, S. S. Sparks, Z. Lyu, A. Pradhan, S. Ding, N. Boddeti, Y. Liu, Y. Lin, D. Du, and K. Qiu, "3D-Printed flexible microfluidic health monitor for in situ sweat analysis and biomarker detection," *ACS Sens.* **9**, 3212 (2024).
- <sup>7</sup>P. Bollella, S. Sharma, A. E. G. Cass, F. Tasca, and R. Antiochia, "Minimally invasive glucose monitoring using a highly porous gold microneedles-based biosensor: Characterization and application in artificial interstitial fluid," *Catalysts* **9**(7), 580 (2019).
- <sup>8</sup>F. Sanai, A. S. Sahid, J. Huvanandana, S. Spoa, L. H. Boyle, J. Hribar, D. T. Y. Wang, B. Kwan, S. Colagiuri, S. J. Cox, and T. J. Telfer, "Evaluation of a continuous blood glucose monitor: A novel and non-invasive wearable using bioimpedance technology," *J. Diabetes Sci. Technol.* **17**(2), 336–344 (2023).
- <sup>9</sup>J. Huang, Y. Zhang, and J. Wu, "Review of non-invasive continuous glucose monitoring based on impedance spectroscopy," *Sens. Actuators, A* **311**, 112103 (2020).
- <sup>10</sup>C. E. F. Amaral and B. Wolf, "Effects of glucose in blood and skin impedance spectroscopy," in *AFRICON 2007* (IEEE, 2007), pp. 1–7.
- <sup>11</sup>R. Pradhan, A. Mitra, and S. Das, "Quantitative evaluation of blood glucose concentration using impedance sensing devices," *J. Electr. Bioimpedance* **4**(1), 73–77 (2013).
- <sup>12</sup>N. D. Nanayakkara, S. C. Munasingha, and G. P. Ruwanpathirana, "Non-invasive blood glucose monitoring using a hybrid technique," in *2018 Moratuwa Engineering Research Conference (MERCon)* (IEEE, 2018), pp. 7–12.
- <sup>13</sup>A. Caduff, M. S. Talary, M. Mueller, F. Dewarrat, J. Klisic, M. Donath, L. Heinemann, and W. A. Stahel, "Non-invasive glucose monitoring in patients with type 1 diabetes: A multisensor system combining sensors for dielectric and optical characterisation of skin," *Biosens. Bioelectron.* **24**(9), 2778–2784 (2009).
- <sup>14</sup>A. Caduff, M. Mueller, A. Megej, F. Dewarrat, R. E. Suri, J. Klisic, M. Donath, P. Zakharov, D. Schaub, W. A. Stahel, and M. S. Talary, "Characteristics of a multisensor system for non invasive glucose monitoring with external validation and prospective evaluation," *Biosens. Bioelectron.* **26**(9), 3794–3800 (2011).
- <sup>15</sup>I. Guyon and A. Elisseeff, "An introduction to variable and feature selection," *J. Mach. Learn. Res.* **3**, 1157–1182 (2003).
- <sup>16</sup>C. T. Yen, U. H. Chen, G. C. Wang, and Z. X. Chen, "Non-invasive blood glucose estimation system based on a neural network with dual-wavelength photoplethysmography and bioelectrical impedance measuring," *Sensors* **22**(12), 4452 (2022).
- <sup>17</sup>K. D. Pathirage, P. Roopasinghe, J. J. Sooriyaarachchi, R. Weththasinghe, and N. D. Nanayakkara, "Removing subject dependencies on non-invasive blood glucose measurement using hybrid techniques," in *2019 41st Annual International Conference of the IEEE Engineering in Medicine and Biology Society (EMBC)* (IEEE, 2019), pp. 7197–7200.
- <sup>18</sup>U. G. Kyle, I. Bosaeus, A. D. De Lorenzo, P. Deurenberg, M. Elia, J. M. Gomez, B. L. Heitmann, L. K. Smith, J. C. Melchior, M. Pirlich *et al.*, "Bioelectrical impedance analysis—Part I: Review of principles and methods," *Clin. Nutr.* **23**(5), 1226–1243 (2004).
- <sup>19</sup>C. Margo, J. Katrib, M. Nadi, and A. Rouane, "A four-electrode low frequency impedance spectroscopy measurement system using the AD5933 measurement chip," *Physiol. Meas.* **34**(4), 391 (2013).
- <sup>20</sup>I. Harman-Boehm, A. Gal, A. M. Raykhman, J. D. Zahn, E. Naidis, and Y. Mayzel, "Noninvasive glucose monitoring: A novel approach," *J. Diabetes Sci. Technol.* **3**, 253 (2009).
- <sup>21</sup>I. Ermolina, Y. Polevaya, and Y. Feldman, "Analysis of dielectric spectra of eukaryotic cells by computer modeling," *Eur. Biophys. J.* **29**, 141–145 (2000).
- <sup>22</sup>D. A. Dean, T. Ramanathan, D. Machado, and R. Sundararajan, "Electrical impedance spectroscopy study of biological tissues," *J. Electrostat.* **66**(3–4), 165–177 (2008).
- <sup>23</sup>Y. Liu, M. Xia, Z. Nie, J. Li, Y. Zeng, and L. Wang, "In vivo wearable non-invasive glucose monitoring based on dielectric spectroscopy," in *2016 IEEE 13th International Conference on Signal Processing (ICSP)* (IEEE, 2016), pp. 1388–1391.
- <sup>24</sup>R. Takamatsu, K. Higuchi, and D. Muramatsu, "Measurement frequency evaluation for bioimpedance-based blood-glucose estimation," in *2021 IEEE 3rd Global Conference on Life Sciences and Technologies (LifeTech)* (IEEE, 2021), pp. 309–310.
- <sup>25</sup>K. Chinen, I. Kinjo, A. Zamami, K. Irei, and K. Nagayama, "New equivalent-electrical circuit model and a practical measurement method for human body impedance," *Bio-Med. Mater. Eng.* **26**, S779–S786 (2015).
- <sup>26</sup>E. Hernández-Balaguera, E. López-Dolado, and J. L. Polo, "Obtaining electrical equivalent circuits of biological tissues using the current interruption method, circuit theory and fractional calculus," *RSC Adv.* **6**(27), 22312–22319 (2016).

- <sup>27</sup>D. K. Kamat, D. Bagul, and P. M. Patil, "Blood glucose measurement using bioimpedance technique," *Adv. Electron.* **2014**, 1.
- <sup>28</sup>M. Shokrehkhodaei and S. Quinones, "Review of non-invasive glucose sensing techniques: Optical, electrical and breath acetone," *Sensors* **20**(5), 1251 (2020).
- <sup>29</sup>M. Y. Jaffrin and H. Morel, "Body fluid volumes measurements by impedance: A review of bioimpedance spectroscopy (BIS) and bioimpedance analysis (BIA) methods," *Med. Eng. Phys.* **30**(10), 1257–1269 (2008).
- <sup>30</sup>S. Mabrouk, S. Hersek, H. K. Jeong, D. Whittingslow, V. G. Ganti, P. Wolkoff, and O. T. Inan, "Robust longitudinal ankle edema assessment using wearable bioimpedance spectroscopy," *IEEE Trans. Biomed. Eng.* **67**(4), 1019–1029 (2020).
- <sup>31</sup>O. G. Martinsen and A. Heiskanen, *Bioimpedance and Bioelectricity Basics* (Elsevier, 2023).
- <sup>32</sup>R. Tibshirani, "Regression shrinkage and selection via the lasso," *J. R. Stat. Soc. Ser. B: Stat. Methodol.* **58**(1), 267–288 (1996).
- <sup>33</sup>M. Zanon, G. Sparacino, A. Facchinetto, M. Riz, M. S. Talary, R. E. Suri, A. Caduff, and C. Cobelli, "Non-invasive continuous glucose monitoring: Improved accuracy of point and trend estimates of the multisensor system," *Med. Biol. Eng. Comput.* **50**, 1047–1057 (2012).
- <sup>34</sup>M. Zanon, G. Sparacino, A. Facchinetto, M. S. Talary, A. Caduff, and C. Cobelli, "Regularised model identification improves accuracy of multisensor systems for noninvasive continuous glucose monitoring in diabetes management," *J. Appl. Math.* **2013**, 1.
- <sup>35</sup>M. Yuan and Y. Lin, "Model selection and estimation in regression with grouped variables," *J. R. Stat. Soc. Ser. B: Stat. Methodol.* **68**(1), 49–67 (2006).
- <sup>36</sup>J. Huang and T. Zhang, "The benefit of group sparsity," *Ann. Stat.* **38**, 1978 (2010).
- <sup>37</sup>J. Friedman, T. Hastie, and R. Tibshirani, "A note on the group lasso and a sparse group lasso," *arXiv:1001.0736* (2010).
- <sup>38</sup>N. Simon, J. Friedman, T. Hastie, and R. Tibshirani, "A sparse-group lasso," *J. Comput. Graphical Stat.* **22**(2), 231–245 (2013).
- <sup>39</sup>K. Song, U. Ha, S. Park, J. Bae, and H. J. Yoo, "An impedance and multi-wavelength near-infrared spectroscopy IC for non-invasive blood glucose estimation," *IEEE J. Solid-State Circuits* **50**(4), 1025–1037 (2015).
- <sup>40</sup>A. Caduff and M. Talary, "Glucose detection from skin dielectric measurement," in *Dielectric Relaxation in Biological Systems* (Oxford University Press, Oxford, 2015), pp. 388–412.
- <sup>41</sup>M. Zanon, M. Mueller, P. Zakharov, M. S. Talary, M. Donath, W. A. Stahel, and A. Caduff, "First experiences with a wearable multisensor device in a noninvasive continuous glucose monitoring study at home, part II: The investigators' view," *J. Diabetes Sci. Technol.* **12**(3), 554–561 (2018).
- <sup>42</sup>W. L. Clarke, D. Cox, L. A. Gonter-Frederick, W. Carter, and S. L. Pohl, "Evaluating clinical accuracy of systems for self-monitoring of blood glucose," *Diabetes Care* **10**(5), 622–628 (1987).
- <sup>43</sup>H. Crandall, A. Burt, and B. Sanchez, "Characterization of the analog device inc (ADI) MAX30009 bioimpedance analog front end chip," in *2022 44th Annual International Conference of the IEEE Engineering in Medicine & Biology Society (EMBC)* (IEEE, 2022), pp. 2502–2505.
- <sup>44</sup>Z. Wang, X. Xiao, C. Yang, and T. Kikkawa, "Combined approach to estimate blood glucose level in noninvasive monitoring: Ultra-wide band microwave and cascaded general regression neural network," *IEEE Trans. Ind. Inf.* **18**(8), 5105–5114 (2022).
- <sup>45</sup>M. H. Chowdhury, M. E. H. Chowdhury, and A. Alqahtani, "MMG-net: Multi modal approach to estimate blood glucose using multi-stream and cross modality attention," *Biomed. Signal Process. Control* **92**, 105975 (2024).